ISSN 1070-3284, Russian Journal of Coordination Chemistry, 2019, Vol. 45, No. 10, pp. 712–720. © Pleiades Publishing, Ltd., 2019.
Russian Text © The Author(s), 2019, published in Koordinatsionnaya Khimiya, 2019, Vol. 45, No. 10, pp. 617–626.

Polynuclear Heteroligand Yb(III)–Er(III) Complexes as Potential Upconversion Materials

T. V. Balashova[a], *, E. V. Baranov[a], G. K. Fukin[a], V. A. Ilichev[a], I. D. Grishin[b], A. N. Yablonskiy[b], [c], B. A. Andreev[b], [c], and M. N. Bochkarev[a], [b]

[a] *Razuvaev Institute of Organometallic Chemistry, Russian Academy of Sciences, Nizhny Novgorod, 603950 Russia*
[b] *Lobachevsky State University of Nizhny Novgorod, Nizhny Novgorod, 603950 Russia*
[c] *Institute for Physics of Microstructures, Russian Academy of Sciences, Nizhny Novgorod, 603950 Russia*
**e-mail: petrovsk@iomc.ras.ru*

Received March 27, 2019; revised April 4, 2019; accepted April 10, 2019

Abstract—The synthesis of complexes $LnI(C_6F_5O)_2$ and $LnCp(L)_2$ (Ln = Er, Yb; L = C_6F_5O, SON^F), which are convenient precursors for the preparation of heteroligand bimetallic complexes, is described. The structures of $YbI(C_6F_5O)_2(DME)_2$ (**I**), $CpEr(C_6F_5O)_2(DME)[(C_2H_5)_2O]$ (**III**), and $CpYb(SON^F)_2(DME)$ (**VI**) were established by X-ray diffraction (CIF files CCDC (nos. 1902963 (**I**), 1902964 (**III**), and 1902965 (**VI**)). The developed methods were used to prepare heteroligand bimetallic Yb(III)–Er(III) complexes $(C_6F_5O)_2Yb[\mu\text{-}(CF_3)_2CHO]_2Er(C_6F_5O)_2$ and $\{(SON^F)_2Yb[\mu\text{-}(CF_3)_2CHO]_2\text{-}Er(SON^F)_2\}_x$, which showed metal-centered emission inherent in Yb^{3+} and Er^{3+} ions λ_{em} = 985 and 1540 nm, respectively. This suggests that the obtained compounds can serve as promising upconversion materials.

Keywords: lanthanide, photoluminescence, upconversion, metal-centered emission

DOI: 10.1134/S107032841909001X

INTRODUCTION

A relevant task of the modern medicine and biology is the search for new luminescent materials for biovisualization and diagnosis. Virtually all biomarkers currently used for this purpose have a classical luminescence mechanism: the emission wavelength is greater than the excitation wavelength (normal Stokes shift) [1, 2]. This scheme accounts for a number of drawbacks of luminophores in biomedical applications (invasive short-wavelength radiation, low contrast, masking background luminescence), which are not inherent in the use of upconversion luminophores (anti-Stokes shift emitters) [3]. Now there are virtually no biomarkers that can utilize infrared excitation; this restricts the possibility of studying biological processes at the cellular level and within biological tissues [3, 4]. Indeed, one of the transparency windows of biological tissues is the 700–1200 nm spectral range; therefore, infrared radiation penetrates deep into biological tissues, without damaging the tissue, giving idle luminescence, or affecting biochemical processes and, hence, it does not disturb the natural metabolism. The large wavelength shift between the excitation and upconversion luminescence bands and also high photostability allow tracing single particles and prolonged examination. The advantages of upconversion materials also include long luminescence lifetime. Experimental and theoretical studies of upconversion processes and development of the scientific methodology are highly relevant for the development of biolabels, which would enhance the quality and depth of visualization of biological objects. Lanthanide ions with abundant luminescence-active transitions in a broad spectral range and two and more metastable states are widely used for this purpose. Since ytterbium ion has a large effective absorption cross-section in the IR region, it is promising as a sensitizing ion. [4]. Erbium ion, which has a long lifetime of excited metastable states to which energy is transferred, is often used as the emission center [5–7]. It is known that the presence of high-energy C–H and O–H bonds in the coordination environment of the lanthanide ion leads to nonradiative relaxation, which decreases the efficiency of energy transfer; as a consequence, luminescence intensity and the excited state lifetime decrease. The replacement of C–H bonds by C–F bonds is an efficient strategy for the synthesis of new IR luminescent Ln^{+3} complexes [8–11].

Despite the advantages of upconversion materials with organic ligands, there are only few such systems [12, 13] because of difficulty of their preparation. It was of interest to prepare an organic lanthanide material exhibiting an anti-Stokes shift with *f*–*f* transition-based luminescence.

EXPERIMENTAL

The syntheses were carried out under conditions excluding contact with oxygen or air moisture using standard Schlenk technique. Diethyl ether, tetrahydrofuran (THF), and dimethoxyethane (DME) were dried with sodium benzophenone ketyl, while hexane and pentane were dried over sodium by standard procedures and withdrawn in vacuo immediately prior to use. The silylamide $Ln[N(SiMe_3)_2]_3$ and cyclopentadienyl $(Cp)_3Ln$ complexes were prepared by reported procedures [14–16]. The 2-(3,4,5,6-tetrafluoro-2-hydrophenyl)-4,5,6,7-tetrafluorobenzothiazole ligand $[H(SON^F)]$ was obtained by procedure [17].

Synthesis of $YbI(C_6F_5O)_2(DME)_2$ (I). A solution of pentafluorophenol (165 mg, 0.89 mmol) in DME (10 mL) was added to a solution of Cp_2YbI (145 mg, 0.79 mmol) in DME (5 mL). The reaction mixture was stirred for 30 min at room temperature. Upon slow removal of volatile reaction products, orange crystals precipitated. The yield of **I** was 263 mg (79%).

For $C_{20}H_{20}O_6F_{10}IYb$

Anal. calcd., %	C, 28.38	H, 2.38	Yb, 20.45
Found, %	C, 28.31	H, 2.39	Yb, 20.49

IR (KBr; ν, cm^{-1}): 3670 w, 3384 w, 2728 w, 2675 w, 2469 w, 2159 w, 2079 s, 1656 w, 1632 w, 1516 s, 1313 w, 1250 w, 1167 m, 1018 s, 997 s, 634 w, 571 w.

Synthesis of $ErI(C_6F_5O)_2(DME)_2$ (II) was carried out similarly to the synthesis of **I** from pentafluorophenol (97 mg, 0.52 mmol) and Cp_2ErI (112 mg, 0.26 mmol) in a DME solution. The yield was 184 mg (83%).

For $C_{20}H_{20}O_6F_{10}IEr$

Anal. calcd., %	C, 28.58	H, 2.40	Er, 19.90
Found, %	C, 28.55	H, 2.43	Er, 19.96

The IR spectrum of complex **II** was similar to the spectrum of **I**.

Synthesis of $CpEr(C_6F_5O)_2(DME)[(C_2H_5)_2O]$ (III). A solution of pentafluorophenol (139 mg, 0.76 mmol) in DME (10 mL) was added to a solution of Cp_3Er (137 mg, 0.38 mmol) in DME (5 mL). The reaction mixture was stirred for 30 min at room temperature and the solvent was removed. The resulting compound was washed with cold hexane and dried in vacuo. The yield of **III**, formed as a light pink powder, was 230 mg (81%). The crystals suitable for X-ray diffraction were obtained by recrystallization of complex **III** from a DME–diethyl ether solvent mixture (1 : 1).

For $C_{25}H_{25}O_5F_{10}Er$

Anal. calcd., %	C, 39.42	H, 3.18	Er, 21.96
Found, %	C, 39.49	H, 3.14	Er, 22.04

IR (KBr; ν, cm^{-1}): 3658 w, 3607 w, 1651 m, 1510 s, 1309 m, 1245 m, 1179 m, 1098 w, 1047 m, 1017 s, 990 s, 861 m, 786 m, 636 w, 465 w, 417 w.

Synthesis of $CpYb(C_6F_5O)_2(DME)[(C_2H_5)_2O]$ (IV) was carried out similarly to the synthesis of **III** from pentafluorophenol (139 mg, 0.75 mmol) and Cp_3Yb (137 mg, 0.38 mmol) in a DME solution. The yield was 235 mg (86%).

For $C_{25}H_{24}O_5F_{10}Yb$

Anal. calcd., %	C, 39.12	H, 3.15	Yb, 22.55
Found, %	C, 39.17	H, 3.20	Yb, 22.59

The IR spectrum of complex **IV** was similar to the spectrum of compound **III**.

Synthesis of $(C_6F_5O)_2Yb[\mu\text{-}(CF_3)_2CHO]_2Er\text{-}(C_6F_5O)_2$ (V). A solution of 1,1,1,3,3,3-hexafluoropropan-2-ol (77 mg, 0.46 mmol) in THF (10 mL) was added to a solution of $CpEr(C_6F_5O)_2$ (169 mg, 0.23 mmol) and $CpYb(C_6F_5O)_2$ (162 mg, 0.23 mmol) in THF (10 mL). The reaction mixture was stirred for 30 min at room temperature and the solvent was removed. The solid residue was washed with cold hexane and dried in vacuo. The yield of **V**, formed as an orange powder, was 202 mg (63%).

For $C_{30}H_2O_6F_{32}YbEr$

Anal. calcd., %	C, 25.62	H, 0.14
Found, %	C, 25.67	H, 0.18

Synthesis of $CpYb(SON^F)_2(DME)$ (VI). A solution of $H(SON^F)$ (103 mg, 0.28 mmol) in DME (10 mL) was added to a solution of Cp_3Yb (51 mg, 0.14 mmol) in DME (5 mL). The reaction mixture was stirred for 30 min at room temperature and the solvent was removed. The resulting compound was washed with cold hexane and dried in vacuo. The yield of **VI**, formed as red-yellow crystals, was 27 mg (33%).

For $C_{35}H_{15}N_2O_4F_{16}S_2Yb$

Anal. calcd., %	C, 39.34	H, 1.41	N, 2.62	S, 6.00	Yb, 16.19
Found, %	C, 39.40	H, 1.48	N, 2.57	S, 6.05	Yb, 16.23

IR (KBr; ν, cm^{-1}): 1642 w, 1098 m, 1050 m, 991 m, 886 m, 790 m.

Synthesis of $CpEr(SON^F)_2(DME)$ (VII). A solution of $H(SON^F)$ (86 mg, 0.23 mmol) in DME (10 mL) was added to a solution of Cp_3Er (42 mg, 0.12 mmol) in DME (5 mL). The reaction mixture was stirred for 30 min at room temperature and the solvent was removed. The resulting compound was washed with cold hexane and dried in vacuo. The yield of **VII**, formed as yellow crystals, was 75 mg (62%).

For $C_{35}H_{15}F_{16}N_2O_4S_2Er$

Anal. calcd., %	C, 39.55	H, 1.42	N, 2.64	S, 6.03	Er, 15.74
Found, %	C, 39.47	H, 1.48	N, 2.70	S, 6.06	Er, 15.69

The IR spectrum of **VII** was identical to the spectrum of compound **VI**.

Synthesis of $\{(SON^F)_2Er[\mu\text{-}(CF_3)_2CHO]_2Yb(SON^F)_2\}_x$ (VIII). A solution of 1,1,1,3,3,3-hexafluoropropan-2-ol (15 mg, 0.089 mmol) in DME (10 mL) was added to a solution of $CpEr(SON^F)_2$ (48 mg, 0.044 mmol) and $CpYb(SON^F)_2$ (48 mg, 0.044 mmol) in DME (10 mL). The reaction mixture was stirred for 30 min at room temperature and the solvent was removed. The solid residue was washed with cold hexane and dried in vacuo. The yield of **VIII**, formed as a light yellow powder, was 64 mg (61%).

For $C_{58}H_2N_4O_6F_{44}S_4YbEr$

Anal. calcd., %	C, 32.32	H, 0.09	N, 2.60
Found, %	C, 32.34	H, 0.10	N, 2.54

IR (KBr; ν, cm^{-1}): 3640 w, 1744 w, 1651 m, 1581 m, 1509 s, 1421 s, 1350 m, 1291 m, 1262 s, 1187 s, 1100 s, 1054 s, 996 s, 885 m, 818 m, 752 m, 652 w, 600 w, 524 w, 498 w.

IR spectra were measured on an FSM-1201 Fourier transform spectrometer in the 4000–400 cm^{-1} range (mineral oil mulls). Elemental analysis for C, H, N, S was performed on an Elementar Vario ELcube Analyzer. The photoluminescence (PL) spectra in the visible and IR regions were measured on USB2000 and NIR-512 spectrometers (Ocean Optics) upon excitation with diode lasers at 405, 940, and 980 nm.

Time-resolved photoluminescence (PL) spectroscopy was used. The PL and PL excitation spectra were studied with pulse excitation of solid samples (T = 298 K) using an MOPO-SL optical parametric oscillator (Spectra-Physics). The wavelength was adjusted in the spectral range of 750–1100 nm, with the pulse duration being 5 ns and the repetition frequency being 10 Hz. The PL spectra in the near-IR range (0.8–1.6 μm) were recorded using an Acton-2300i grating monochromator and a Hamamatsu H10330A-75 photocell multiplier.

Mass spectra were run on a Bruker Microflex LT mass spectrometer in the linear mode. The sample preparation was as follows: 2–5 mg of a solid compound was spread over a stainless-steel plate with a spatula. A solution (2 μL) of DCTB (*trans*-2-[3-(4-*tert*-butylphenyl)-2-methyl-2-propenylidene]malononitrile) (20 mg/mL) in THF was applied onto the spread compound and then the sample was dried in air for 5–10 s and placed into the spectrometer. Positive- or negative-ion spectra were recorded depending on the particular compound.

X-ray diffraction study of complexes **I**, **III**, and **VI** was carried out on Bruker D8 Quest (**I**, **III**) and Oxford Xcalibur Eos (**VI**) automated diffractometers (graphite monochromator, MoK_α-radiation, and φ- and ω-scan techniques, λ = 0.71073 Å). The experimental sets of reflection intensities were integrated using SAINT software [18] for **I** and **III** and CrysAlisPro [19] for **VI**. The SADABS [20] (**I**, **III**) and SCALE3 ABSPACK (**VI**) [21] programs were used to apply absorption corrections. The structures were solved by the dual-space method with the SHELXT program [22]. Nonhydrogen atoms were refined by full-matrix least-squares method on F^2_{hkl} in the anisotropic approximation using the SHELXTL software [23]. Hydrogen atoms were placed in geometrically calculated positions and refined in the riding model. The crystal of complex **VI** is a racemic twin with a domain ratio of 0.48 : 0.52. The chelating SON^F ligands of complex **VI** are disordered over two positions. The key crystallographic characteristics and X-ray experiment details for **I**, **III**, and **VI** are summarized in Table 1.

The structures are deposited with the Cambridge Crystallographic Data Centre (nos. 1902963 (**I**), 1902964 (**III**), and 1902965 (**VI**); deposit@ccdc.cam.ac.uk or http://www.ccdc.cam.ac.uk/data_request/cif).

RESULTS AND DISCUSSION

Previously, the upconversion phenomenon was observed for the Yb(III)–Et(III) hexafluoroisopropoxide complex, $Er_{0.67}Yb_{1.33}[(CF_3)_2CHO]_9$ [13]. In order to prepare more efficient upconversion materials, here we attempted to synthesize heteroligand bimetallic lanthanide complexes.

In the first stage, we prepared ytterbium and erbium heteroligand complexes, which were subsequently used as precursors for the synthesis of heteroligand bimetallic compounds. The reaction of Cp_2YbI with pentafluorophenol in 1 : 2 molar ratio in a DME solution gave complex **I**. The compound was isolated as orange crystals in 76% yield. According to X-ray diffraction, the ytterbium atom in complex **I** is bound to two pentafluorophenolate ligands, iodine atom, and two DME molecules (Fig. 1). Atom (1) has a distorted one-capped trigonal prism configuration (coordination number of Yb is 7). The rings of pentafluorophenolate ligands are located virtually in parallel planes (the dihedral angle between the planes is 7.4°). Erbium complex **II** was prepared in a similar way.

Complex **III** was obtained by the reaction of Cp_3Er with pentafluorophenol in 1 : 2 molar ratio in DME and isolated in 81% yield. The formation of

Table 1. Crystallographic data and structure refinement details for complexes **I**, **III**, and **VI**

Parameter	Value		
	I	**III**	**VI**
Molecular Formula	$C_{20}H_{20}O_6F_{10}IYb$	$C_{25}H_{25}O_5F_{10}Er$	$C_{35}H_{15}N_2O_4F_{16}S_2Yb$
M	846.30	762.71	1068.65
Temperature, K	100(2)	100(2)	100(2)
System	Triclinic	Monoclinic	Orthorhombic
Space group	$P\bar{1}$	$P2_1/n$	$Pca2_1$
Unit cell parameters:			
a, Å	9.8273(7)	13.6792(4)	15.4140(3)
b, Å	11.2936(8)	10.6054(3)	10.7544(1)
c, Å	12.4865(9)	18.2013(5)	41.5039(6)
α, deg	93.211(4)	90	90
β, deg	94.319(3)	91.9799(11)	90
γ, deg	112.935(3)	90	90
V, Å^3	1267.13(16)	2638.95(13)	6880.03(18)
Z	2	4	8
ρ(calcd.), mg/m^3	2.218	1.920	2.063
μ, mm^{-1}	5.016	3.286	2.973
Crystal size, mm	0.30 × 0.12 × 0.02	0.32 × 0.26 × 0.18	0.37 × 0.35 × 0.26
F(000)	802	1492	4136
θ Range of measurements, deg	2.34–28.00	2.22–32.58	3.03–28.70
Number of reflections collected/unique	13889/6101	43097/9618	115127/17770
R_{int}	0.0313	0.0288	0.0647
Number of reflections with $I > 2\sigma(I)$	5519	8793	15954
R_1, wR_2 ($I > 2\sigma(I)$)	0.0252, 0.0615	0.0202, 0.0463	0.0574, 0.1036
R_1, wR_2 (for all data)	0.0302, 0.0631	0.0238, 0.0474	0.0643. 0.1073
S	1.047	1.082	1.065
Absolute structural parameter			0.48(2)
Residual electron density (max/min), e/Å^3	1.421/–1.633	1.725/–1.074	2.026/–5.280

compound **III** was confirmed by elemental analysis and IR spectroscopy. According to X-ray diffraction data, in **III**, the erbium ion is linked to two pentafluorophenolate and one cyclopentadienyl ligands and to DME and diethyl ether molecules (Fig. 2). The Er(1) coordination polyhedron is a distorted octahedron, with the base being formed by the O(1–4) atoms of the pentafluorophenolate and DME ligands and axial positions being occupied by the Cp ligand and the diethyl ether O(5) atom. The sum of angles in the equatorial plane was ~349°. The Er(1) atom deviates from the octahedron base plane by 0.496(1) Å towards the Cp substituent. The rings of pentafluorophenolate ligands are nearly coplanar, the dihedral angle between their planes being 5.59(6)°. Complex **IV** was prepared in a similar way.

The Yb(III)–Er(III) heteroligand complex **V** was synthesized by the reaction of iodo derivatives $LnI(OC_6F_5)_2$ (Ln = Yb, Er) with potassium hexafluoroisopropoxide taken in 1 : 1 : 2 ratio in a THF solution (Scheme 1).

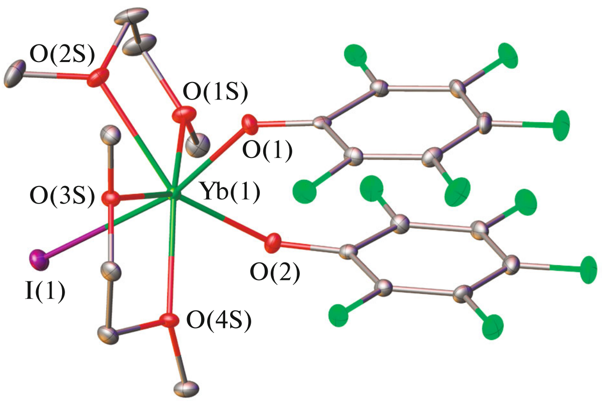

Fig. 1. Molecular structure of complex **I**. Selected distances and angles: Yb(1)–O(1), 2.125(2); Yb(1)–O(2), 2.124(2); Yb(1)–I(1), 3.0309(3); Yb(1)–O(1S–4S), 2.356(2)–2.395(2) Å; and O(1)Yb(1)O(2), 88.23(9)°; O(1)Yb(1)I(1), 166.47(7)°; O(2)Yb(1)I(1), 103.54(6)°; O(1S)Yb(1)O(2S), 67.70(9)°; O(3S)Yb(1)O(4S), 67.38(8)°; O(1S)Yb(1)I(1), 81.22(6)°; O(2S)Yb(1)I(1), 86.35(6)°; O(3S)Yb(1)I(1), 96.13(6)°; O(4S)Yb(1)I(1), 79.83(6)°. The thermal ellipsoids are drawn at the 30% probability level. The hydrogen atoms are omitted.

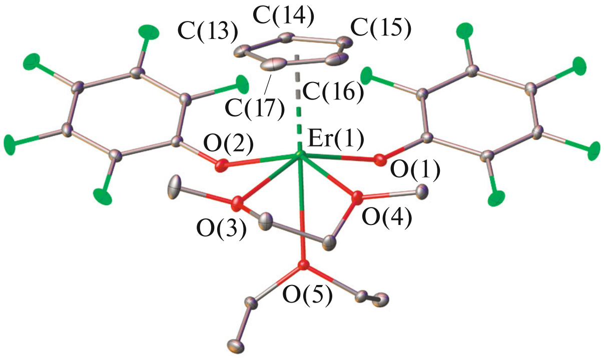

Fig. 2. Molecular structure of complex **III**. Distances and angles: Er(1)–Cp[C(13)–C(17)], 2.3764(8); Er(1)–O(1), 2.1466(12); Er(1)–O(2), 2.1670(11); Er(1)–O(3), 2.4462(12); Er(1)–O(4), 2.3966(11); Er(1)–O(5), 2.4593(11) Å; and O(1)Er(1)O(2), 106.84(5)°; O(2)Er(1)O(3), 86.19(4)°; O(3)Er(1)O(4), 66.00(4)°; O(4)Er(1)O(1), 89.54(4)°; O(2)Er(1)O(4), 146.12(4)°; O(1)Er(1)O(3), 147.52(4)°; Cp[C(13)–C(17)]Er(1)O(5), 176.4(3)°. The thermal ellipsoids are drawn at the 30% probability level. The hydrogen atoms are omitted.

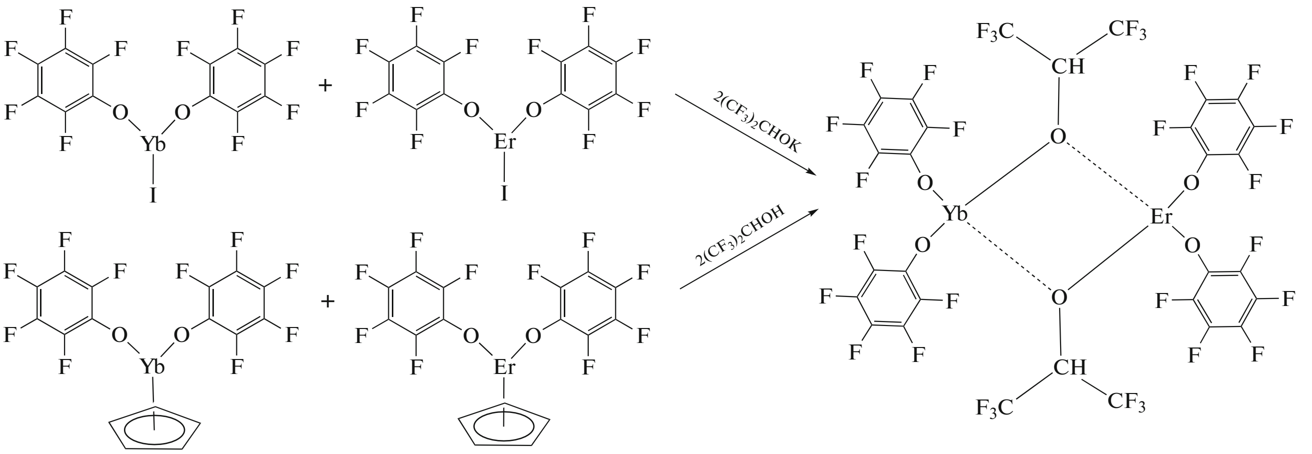

(V)

Scheme 1.

A drawback of this method is the necessity to separate the target reaction product from potassium iodide. Therefore, cyclopentadienyl derivatives such as $CpLn(C_6F_5O)_2$ (Ln = Yb, Er) are more convenient precursors for the synthesis of polynuclear heteroligand complexes. The amount of CpH formed in the reaction was determined by high performance liquid chromatography.

The homoligand $ErYb[(CF_3)_2CHO]_6$ and $ErYb(NpSON)_6$ complexes prepared previously have a dimeric structure with four terminal and two bridging ligands [13]. Since no crystals suitable for X-ray diffraction were obtained for **V**, its structure was suggested relying on the data of elemental analysis, IR spectroscopy, and matrix-assisted laser desorption ionization time-of-flight (MALDI TOF) mass spectrometry. The negative-ion mass spectrum of complex **V** (Fig. 3a) exhibits a signal at 1620 Da, corresponding to superposition of signals of the $Er_2(C_6F_5O)_7O^-$, $YbEr(C_6F_5O)_7^-$, and $Yb_2(C_6F_5O)_7^-$ ions, which confirms the presence of bridged polynuclear structures in the crystal. The signal at 905 Da corresponds to the $Er(C_6F_5O)_4^-$ and $Yb(C_6F_5O)_4^-$ mononuclear anions.

The signal at 1040 Da in the spectrum recorded in the positive ion mode corresponds to superposition of signals of the binuclear species, $Er_2[(CF_3)_2CHO]_2(C_6F_5O)_2^+$, $YbEr[(CF_3)_2CHO]_2(C_6F_5O)_2^+$, and $Yb_2[(CF_3)_2\text{-}CHO]_2(C_6F_5O)_2^+$, containing two different types of ligands. In the mass spectrum, a signal at m/z = 1283 can be

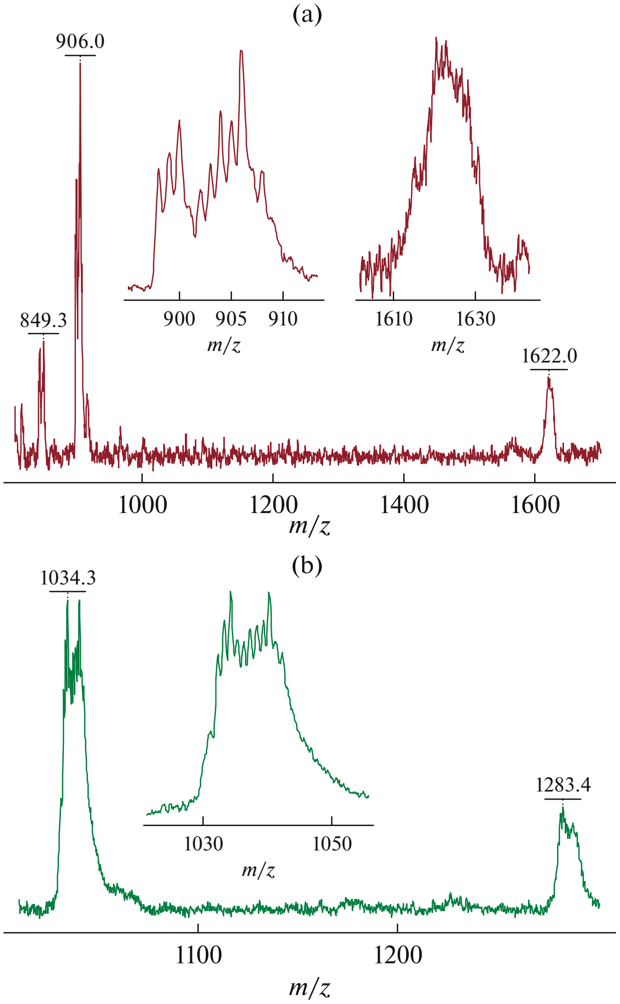

Fig. 3. Mass spectrum of **V** recorded in the (a) negative and (b) positive ion modes with DCTB as the matrix.

detected, which corresponds to superposition of signals of the same ions as adducts with the matrix molecule (DCTB, $C_{17}H_{18}N_2$, $M = 250$) (Fig. 3b). These data of mass spectrometry, together with the elemental analysis data suggest that complex **V** is a polynuclear coordination cluster with the $(C_6F_5O)_2Er[\mu\text{-}(CF_3)_2\text{-}CHO]_2Yb\text{-}(C_6F_5O)_2$ group as the structural block.

Previously, it was found that 2-(2-hydroxyphenyl)benzothiazole ligands efficiently sensitize the luminescence of lanthanide ions [24]. Therefore, according to the chosen strategy of replacement of C–H bonds in the ligands by the C–F bond, H(SON^{F}) served as the terminal ligands for heteroligand bimetallic complexes.

The precursors CpLn(SON^{F})$_2$ (Ln = Yb, Er) were prepared by the reactions of lanthanide cyclopentadienides with H(SON^{F}) in 1 : 2 molar ratio in a DME solution. Complex **VI** was isolated in 63% yield. Compound **VII** was formed as yellow crystals in 62% yield. The formation of complexes **VI** and **VII** was confirmed by elemental analysis, IR spectroscopy, and X-ray diffraction.

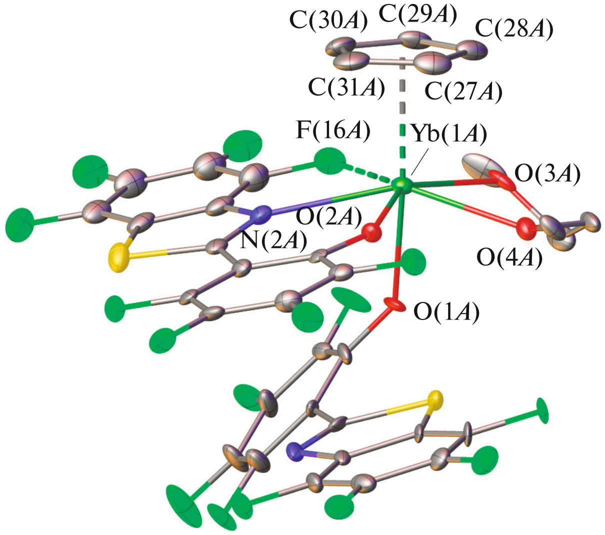

Fig. 4. Structure of molecule A of complex **VI**. Distances and angles (the values are given for molecules A and B, respectively): Yb(1)–Cp[C(27)–C(31)], 2.369(3), 2.340(3); Yb(1)–O(1), 2.210(11), 2.207(10); Yb(1)–O(2), 2.188(15), 2.110(13); Yb(1)–O(3), 2.450(12), 2.411(12); Yb(1)–O(4), 2.389(12), 2.355(11); Yb(1)–N(2), 2.497(14), 2.533(12); Yb(1)–F(16), 2.723(16), 2.791(13) Å; O(2)Yb(1)O(4), 79.2(5)°, 78.7(5)°; O(4)Yb(1)O(3), 67.3(4)°, 68.2(4)°; O(3)Yb(1)F(16), 72.3(4)°, 72.5(4)°; F(16)Yb(1)N(2), 66.2(4)°, 64.4(3)°; N(2)Yb(1)O(2), 70.7(5)°, 71.9(5)°; Cp[C(27)–C(31)]Yb(1)O(1), 171.3(4)°, 163.4(3)°. The thermal ellipsoids are drawn at the 30% probability level. The hydrogen atoms are omitted.

The crystal of **VI** contains two crystallographically independent molecules A and B of Yb complex with identical chemical structure. Complexes **VI** are monomeric, unlike analogous compounds with non-fluorinated ligands, which are dimeric [25]. The ytterbium atom is coordinated by one Cp ligand, two SON^{F} ligands, and one DME molecule (Fig. 4). One of the SON^{F} ligands is monodentately bound to the ytterbium ion, while the other ligand is bidentate. The Yb(1) atom is additionally coordinated to the F(16) atom of the bidentate SON^{F} ligand (Yb(1)···F(16), 2.723(16) and 2.791(13) Å, for molecules A and B, respectively). This contact is a dative C–F → Yb interaction (<3.4 Å [26]). Thus, the Yb(1) atom has a distorted pentagonal bipyramidal environment. The base of the pentagonal bipyramid is formed by bidentate SON^{F} and DME ligands, while the apical positions are occupied by the Cp ligand and the O(1) atom of monodentate SON^{F}. The angle between the axial substituents is 171.3(4)° for A and 163.4(3)° for B, while the sum of angles in the equatorial plane is ~356° in both molecules of complex **VI**.

Similarly to **V**, the binuclear heteroligand complex **VIII** was prepared in 61% yield by the reaction of **VI** and **VII** with hexafluoroisopropanol in 1 : 1 : 2 molar ratio in a DME solution (Scheme 2).

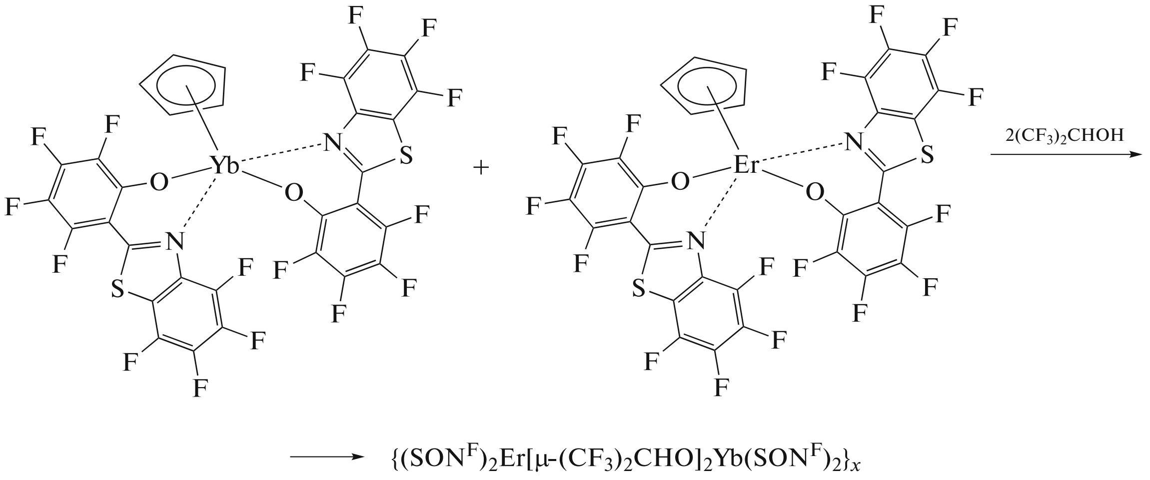

$$\longrightarrow \{(\mathrm{SON^F})_2\mathrm{Er}[\mu\text{-}(\mathrm{CF_3})_2\mathrm{CHO}]_2\mathrm{Yb}(\mathrm{SON^F})_2\}_x$$

Scheme 2.

Like complex **V** considered above, compound **VIII** was isolated from the reaction mixture as a solid whose crystals were unsuitable for X-ray diffraction study. The positive-ion MALDI TOF mass spectrum of this compound exhibits signals for the $\mathrm{Yb(SON^F)_2^+}$ and $\mathrm{Er(SON^F)_2^+}$ mononuclear ions at 905–915 Da and a series of signals for the $\mathrm{(Er,Yb)}_n\mathrm{(SON^F)}_x\text{-}\mathrm{(O,OH)}_y\text{-}\mathrm{((CF_3)_2CHO)}_z^+$ cluster cations in the region of 1.8–6 kDa separated from one another by 556, 184, and 167 Da. This corresponds to the $[\mathrm{(Er,Yb)SON^F + O}]$, $[\mathrm{(CF_3)_2CHO + OH}]$, and $\mathrm{(CF_3)_2CHO}$ fragments, respectively (Fig. 5a). For example, the signal at 3300 Da corresponds to the cation with the formula $\mathrm{(SON^F)_6(Yb,Er)_4(O,OH)_4[(CF_3)_2CHO]_2^+}$. The presence of oxygen atoms and hydroxyl groups is probably due to their formation upon laser-assisted degradation of alcohol residue.

The negative-ion mass spectrum (Fig. 5b) contains signals for mononuclear species such as $\mathrm{(Er,Yb)(SON^F)_3OH^-}$ and $\mathrm{(Er,Yb)(SON^F)_4^-}$ located at 1300 and 1650 Da, respectively, and a number of signals for the anionic clusters above 2700 Da. The distances between these signals are 556 and 351 Da, which corresponds to $[\mathrm{(Er,Yb)SON^F + O}]$ and $\{[\mathrm{(CF_3)_2CHO}]_2 + \mathrm{OH}\}$ fragments and indicates the presence of these fragments in the cluster anions formed in the analysis.

The results suggest that in the crystalline state, compound **VIII** exists as a coordination polymer. According to elemental analysis data, the molecular formula of its structural unit can be represented as $\mathrm{(SON^F)_2Er[\mu\text{-}(CF_3)_2CHO]_2Yb(SON^F)_2}$. On laser treatment, various cluster anions are knocked out from the three-dimensional structure and recorded by the detector. The formation of a complex polymeric structure may be responsible for the difficulty of preparing crystals suitable for crystallography.

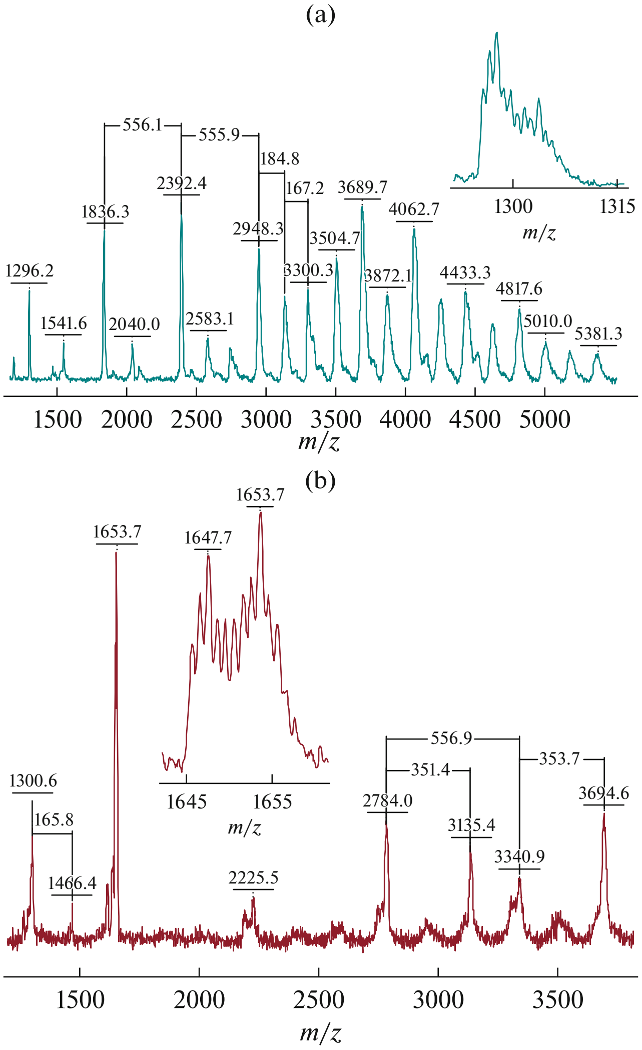

Fig. 5. Mass spectrum of **VIII** recorded in the (a) positive and (b) negative ion modes with DCTB as the matrix.

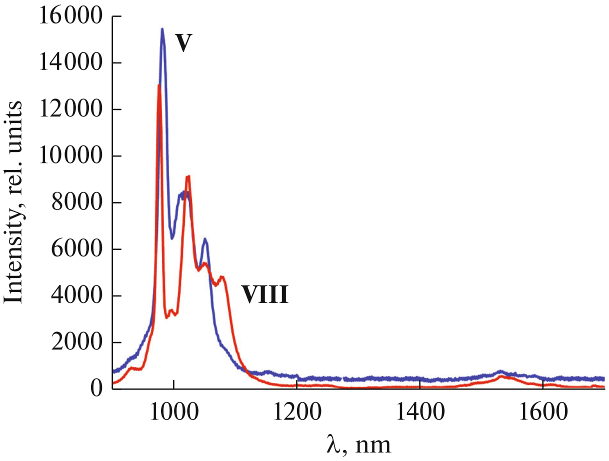

Fig. 6. Photoluminescence spectra in the IR region for complexes **V** and **VIII** upon laser excitation at λ = 405 nm (300 K).

A study of the photoluminescent properties of the complexes demonstrated that diode laser excitation of compounds **V** and **VIII** at λ = 405 nm at 300 K gives rise to intense Yb^{3+} luminescence (985 nm; $^2F_{5/2} \to {}^2F_{7/2}$ transition) and weak Er^{3+} luminescence (λ_{em} of 1540 nm; $^4I_{13/2} \to {}^4I_{15/2}$ transition) (Fig. 6).

The spectra of both **V** and **VIII** display a low-intensity Er^{3+} emission band, which may result from the excitation energy transfer from the ligands or from Yb^{3+} ions. In order to clarify the excitation pattern and to establish the possibility of upconversion for the obtained compounds, the time-resolved PL excitation spectra were studied.

The use of Yb–Er systems to develop upconversion luminophores is based on the energy transfer from the excited $^2F_{5/2}$ level of the ytterbium ion to the $^4I_{11/2}$ metastable level of erbium ion and, further, as the second photon is absorbed, to the excited $^4F_{7/2}$ level, relaxation of which gives a short-wavelength luminescence [27]. Thus, for upconversion to be generated in these systems, it is necessary to provide effective energy transfer from ytterbium to erbium such that a sufficient occupancy of the erbium $^4I_{11/2}$ level is attained. Figure 7 shows the time-resolved PL excitation spectra for compounds **V** and **VIII** (λ_{em} 1540 nm). The excitation spectra of both compounds consist of two bands in the range of 750–1100 nm. The band with a maximum at ~800 nm is evidently caused

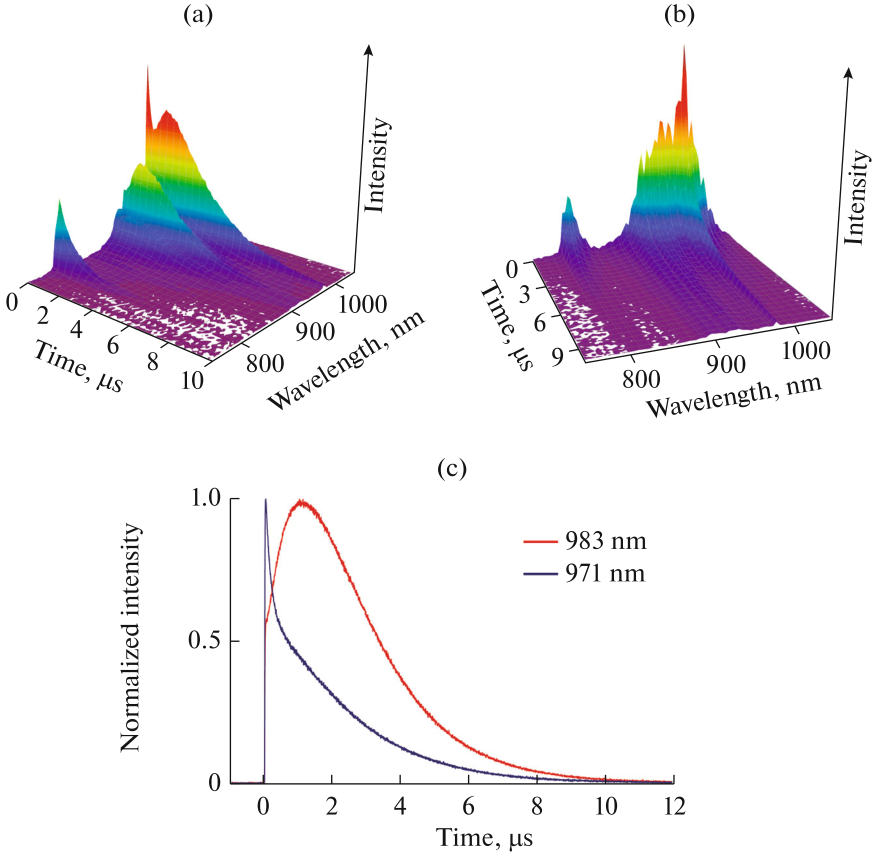

Fig. 7. Time-resolved PL excitation spectrum of (a) complex **V** and (b) **VIII** at λ_{em} = 1540 nm; (c) normalized time profiles of spectrum (a) at excitation wavelengths of 971 and 983 nm.

by the intrinsic $^4I_{15/2} \rightarrow {}^4I_{9/2}$ absorption of the erbium ion. The second band at 900–1000 nm may correspond to both erbium intrinsic absorption ($^4I_{15/2} \rightarrow {}^4I_{11/2}$) and ytterbium absorption ($^2F_{7/2} \rightarrow {}^2F_{5/2}$) followed by energy transfer to erbium. In the PL excitation spectrum of erbium for complex **V** (Fig. 7a), two types of lines are present, some lines with fast rise and decay (λ = 971, 973, and 976 nm) and other lines with a relatively slow rise and slow decay (λ = 978 and 983 nm) (Fig. 7c). Probably, this shape of excitation spectrum is due to superposition of two processes, a fast process comprising energy absorption by the erbium ion ($^4I_{15/2} \rightarrow {}^4I_{11/2}$), nonradiative relaxation to the $^4I_{13/2}$ state, and subsequent emission and a slow process comprising energy absorption by the ytterbium ion, resonance transfer to erbium $^4I_{11/2}$ level with subsequent relaxation and emission. No such peculiar feature was detected in the time-resolved PL excitation spectrum of **VIII** (Fig. 7b), which attests to the absence of energy transfer between two lanthanides in the complex.

It is noteworthy that the increase in the emission intensity at 1540 nm ($^4I_{13/2} \rightarrow {}^4I_{15/2}$ transition of Er^{3+}) occurs over a short period of time, less than 60 ns, for both complexes. This fact attests to the short lifetime and, hence, insufficiently high concentration of the erbium $^4I_{11/2}$ states, which accounts for the absence of upconversion PL for these compounds.

Thus, we synthesized the complexes $LnI(C_6F_5O)_2$ and $LnCp(L)_2$ (Ln = Er, Yb; L = C_6F_5O, SON^F), which are convenient precursors for the preparation of heteroligand bimetallic complexes, and studied their molecular structure by X-ray diffraction. New heterobimetallic complexes, $(C_6F_5O)_2Yb[\mu\text{-}(CF_3)_2CHO]_2\text{-}Er(C_6F_5O)_2$ and $\{(SON^F)_2Er[\mu\text{-}(CF_3)_2CHO]_2Yb\text{-}(SON^F)_2\}_x$, were prepared and studied for luminescent properties. Both compounds exhibited metal-centered emission in the near-IR range caused by *f–f* transitions inherent in the Er^{3+} and Yb^{3+} ions, which enables their use in bioimaging. Currently, attempts are made to modify the ligands in the complexes in order to increase the efficiency of Yb → Er transfer of excitation energy, which is necessary for upconversion to occur.

FUNDING

This work was supported by the Russian Foundation for Basic Research (projects no. 18-33-20103). I.D. Grishin is grateful to the Ministry of Science and Higher Education of the RF (Assignment 4.5630.2017/VU).

CONFLICT OF INTEREST

The authors declare that they have no conflicts of interest.

REFERENCES

1. Auzel, F., *C. R. Seances Acad. Sci., Ser. B*, 1966, vol. 262, p. 1016.
2. Auzel, F., *C. R. Seances Acad. Sci., Ser. B*, 1966, vol. 263, p. 819.
3. Auzel, F., *Chem. Rev.*, 2004, vol. 104, p. 139.
4. Zhou, J., Liu, Q., Feng, W., et al., *Chem. Rev.*, 2015, vol. 115, p. 395.
5. Kanoun, A., Jaba, N., Mejri, H., et al., *Phys. Status Solidi A*, 2001, vol. 188, p. 1145.
6. Vetrone, F., Boyer, J.C., Capobianco, J., et al., *Chem. Mater.*, 2003, vol. 15, p. 2737.
7. Patra, A., Friend, C.S., Kapoor, R., and Prasad, P.N., *Appl. Phys. Lett.*, 2003, vol. 83, p. 284.
8. Glover, P.B., Bassett, A.P., Nockemann, P., et al., *Chem.-Eur. J.*, 2007, vol. 13, p. 6308.
9. Hasegawa, Y., Ohkubo, T., Sogabe, K., et al., *Angew. Chem., Int. Ed. Engl.*, 2000, vol. 39, p. 357.
10. Døssing, A., *Eur. J. Inorg. Chem.*, 2005, vol. 2005, p. 1425.
11. Ilichev, V.A., Silantyeva, L.I., and Yablonskiy, A.N., *Dalton Trans.*, 2019, vol. 48, p. 1060.
12. Sorgho, L.A., Besnard, C., and Pattison, P., *Angew. Chem., Int. Ed. Engl.*, 2011, vol. 50, p. 4108.
13. Balashova, T.V., Pushkarev, A.P., Yablonskiy, A.N., et al., *J. Lumin.*, 2017, vol. 192, p. 208.
14. Bradley, D.C., Ghotra, J.S., and Hart, F.A., *J. Chem. Soc., Dalton Trans.*, 1973, vol. 10, p. 1021.
15. Wilkinson, G. and Birmingham, J.M., *J. Am. Chem. Soc.*, 1954, vol. 76, p. 6210.
16. Birmingham, J.M. and Wilkinson, G., *J. Am. Chem. Soc.*, 1956, vol. 78, p. 42.
17. Li, Z., Dellali, A., Malik, J., Motevalli, M., et al., *Inorg. Chem.*, 2013, vol. 52, p. 1379.
18. *SAINT. Data Reduction and Correction Program*, Version 8.38A, Madison: Bruker AXS Inc., 2017.
19. *Data Collection. Reduction and Correction Program*, CrysalisPro—Software Package Agilent Technologies, 2012.
20. Sheldrick, G.M., *SADABS-2016/2, Bruker/Siemens Area Detector Absorption Correction Program*, Madison: Bruker AXS, 2016.
21. *SCALE3 ABSPACK: Empirical Absorption Correction. CrysAlis Pro—Software Package*, Agilent Technologies, 2012.
22. Sheldrick, G.M., *Acta Crystallogr., Sect. A: Found. Adv.*, 2015, vol. 71, p. 3.
23. Sheldrick, G.M., *SHELXTL. Version 6.14. Structure Determination Software Suite*, Madison: Bruker AXS, 2003.
24. Katkova, M.A., Pushkarev, A.P., Balashova, T.V., et al., *J. Mater. Chem.*, 2011, vol. 21, p. 16611.
25. Pushkarev, A.P., Ilichev, V.A., Balashova, T.V., et al., *Synth. Met.*, 2015, vol. 203, p. 117.
26. Rumyantsev, R.V. and Fukin G.K., *Izv. Akad. Nauk. Ser. Khim.*, 2017, no. 9, p. 1557.
27. Chan, E.M., *Chem. Soc. Rev.*, 2015, vol. 44, p. 1653.

Translated by Z. Svitanko